Supplementary Information for

Cardioprotection by *S*-nitrosation of a cysteine switch on mitochondrial complex I

Edward T. Chouchani[1,2], Carmen Methner[2], Sergiy M. Nadtochiy[3], Angela Logan[1], Victoria R. Pell[2], Shujing Ding[1], Andrew M. James[1], Helena M. Cochemé[1,4], Johannes Reinhold[1], Kathryn S. Lilley[5], Linda Partridge[4], Ian M. Fearnley[1] , Alan J. Robinson[1], Richard C. Hartley[6], Robin A.J. Smith[7], Thomas Krieg[2], Paul S. Brookes[3] & Michael P. Murphy[1]

[1]MRC Mitochondrial Biology Unit, Hills Road, Cambridge CB2 0XY, UK. [2]Department of Medicine, University of Cambridge, Addenbrooke's Hospital, Hills Road, Cambridge, CB2 2QQ, UK. [3]Department of Anesthesiology, University of Rochester Medical Center, 601 Elmwood Avenue, Rochester, NY 14642, USA. [4]Institute of Healthy Ageing, Department of Genetics, Evolution and Environment, University College London, Gower Street, London WC1E 6BT, UK. [5] Department of Biochemistry, Cambridge System Biology Centre, University of Cambridge, Cambridge CB2 1GA, UK. [6]Centre for the Chemical Research of Ageing, WestCHEM School of Chemistry, University of Glasgow, Glasgow, G12 8QQ, UK.[7]Department of Chemistry, University of Otago, P.O. Box 56, Dunedin 9054, New Zealand.

Supplementary Figure 1

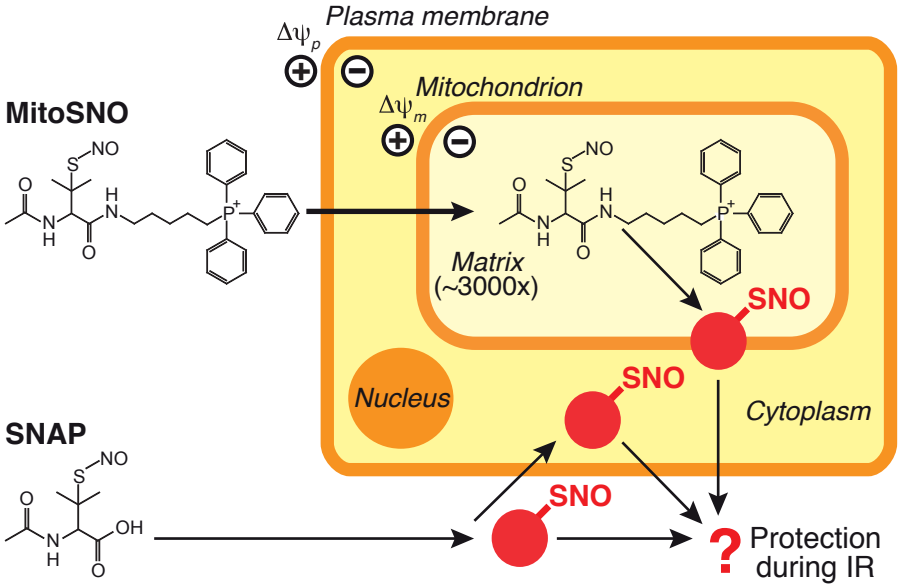

Fig. S1 Selective uptake of MitoSNO into mitochondria *in vivo*.
The lipophilic triphenylphosphonium (TPP) cation component of MitoSNO enables it to be taken up rapidly across biological membranes due to its large ionic radius and hydrophobic surface that lowers its activation energy for movement through a phospholipid bilayer. The extent of uptake is determined by the Nernst equation, and predicts that the uptake should be several thousand-fold. Consequently MitoSNO is accumulated within mitochondria *in vivo* selectively, driven by the large membrane potential across the mitochondrial inner membrane. This selective uptake by MitoSNO should lead to the selective *S*-nitrosation of mitochondrial thiol proteins which may contribute to protection against IR injury *in vivo*. In contrast, the untargeted *S*-nitrosating agent SNAP will only *S*-nitrosate non-mitochondrial proteins. Therefore if the *S*-nitrosation of mitochondrial proteins contributes to protection against IR injury, then MitoSNO should be protective whereas SNAP should not.

Supplementary Figure 2

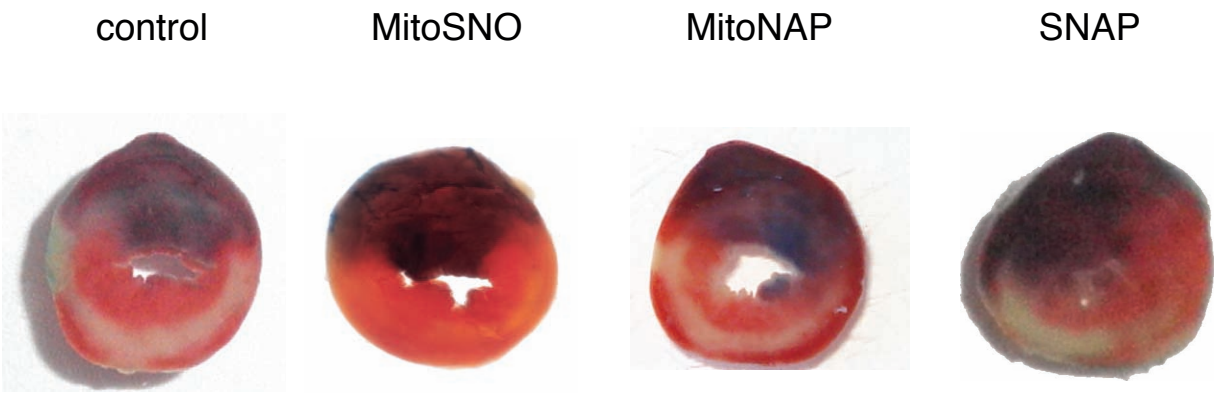

Fig. S2: High resolution representative images of hearts following TTC staining used for infarct quantification in Fig. 1b. Blue staining by Evans Blue dye indicates the non-risk zone. Infarcts are quantified as % TTC stained infarct (white) as a proportion of the at risk zone (non-blue stained). Full experimental details are provided in the supplementary methods section

Supplementary Figure 3

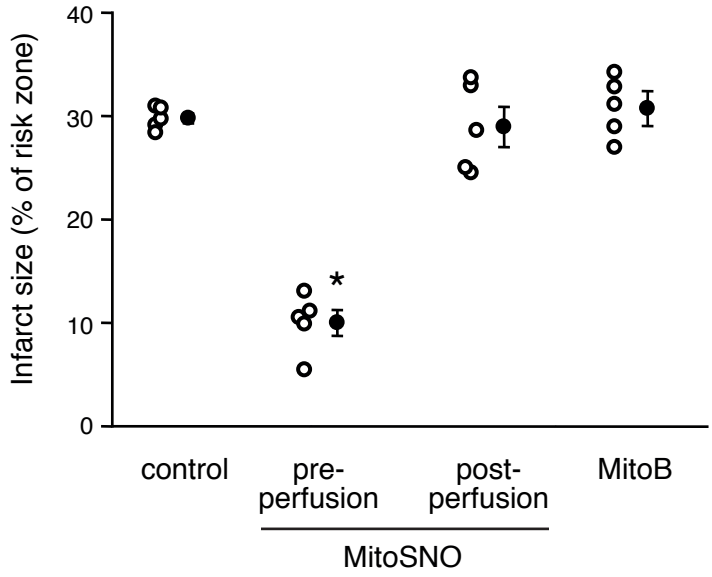

Fig. S3 Injection of MitoSNO post-reperfusion does not protect against IR injury. Cardiac IR injury was generated in mice *in vivo* as described in Fig. 1b. Injection of MitoSNO (100 ng/kg) administered by tail vein IV 5 min before reperfusion was protective against IR injury. However, injection of MitoSNO 10 min after the initiation of reperfusion was not protective. MitoB (3 μmol/kg), injected by IV 1.5 h prior to reperfusion did not affect infarct size. $N \geq 3$ for all groups, * $p < 0.05$ versus control.

Supplementary Figure 4

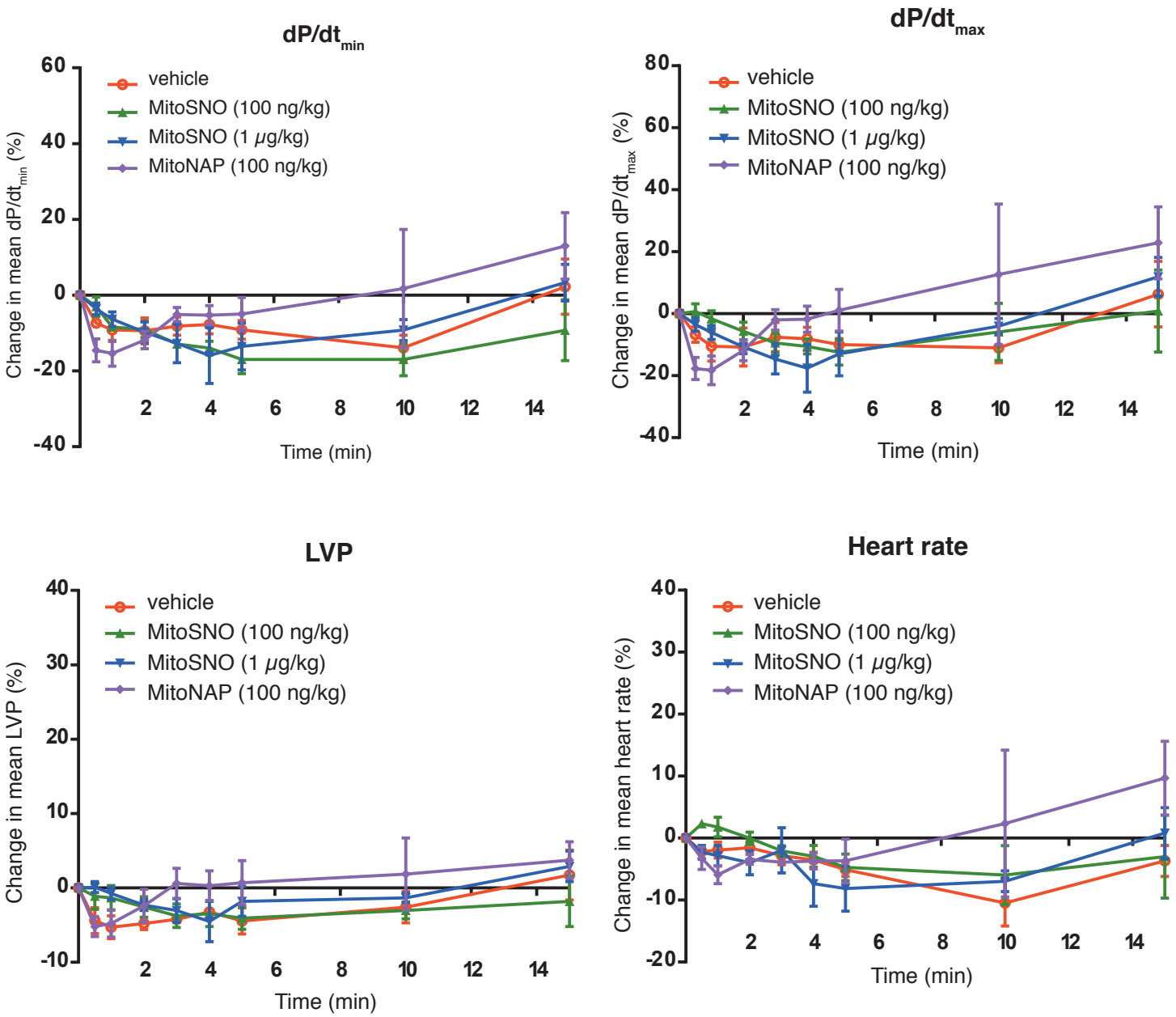

Fig. S4 MitoSNO does not affect hemodynamics

A closed-chest experimental model was used to assess the effect of MitoSNO on hemodynamics. A pressure-conductance catheter was inserted into the right carotid artery and extended into the left ventricle. The effect of intravenous (IV) administration of MitoSNO (100 ng/kg and 1 μg/kg), MitoNAP (100 ng/kg) and vehicle (saline) on the hemodynamic parameters: left ventricular pressure (LVP), heart rate, dP/dt_{max} and dP/dt_{min} were determined. Hemodynamic parameters recovered to equivalent to or above baseline levels 15 min post treatment. There was no significant difference between MitoSNO or MitoNAP in comparison to vehicle at any time point of the experiment in any of the parameters measured. N = 3 for each group.

Supplementary Figure 5

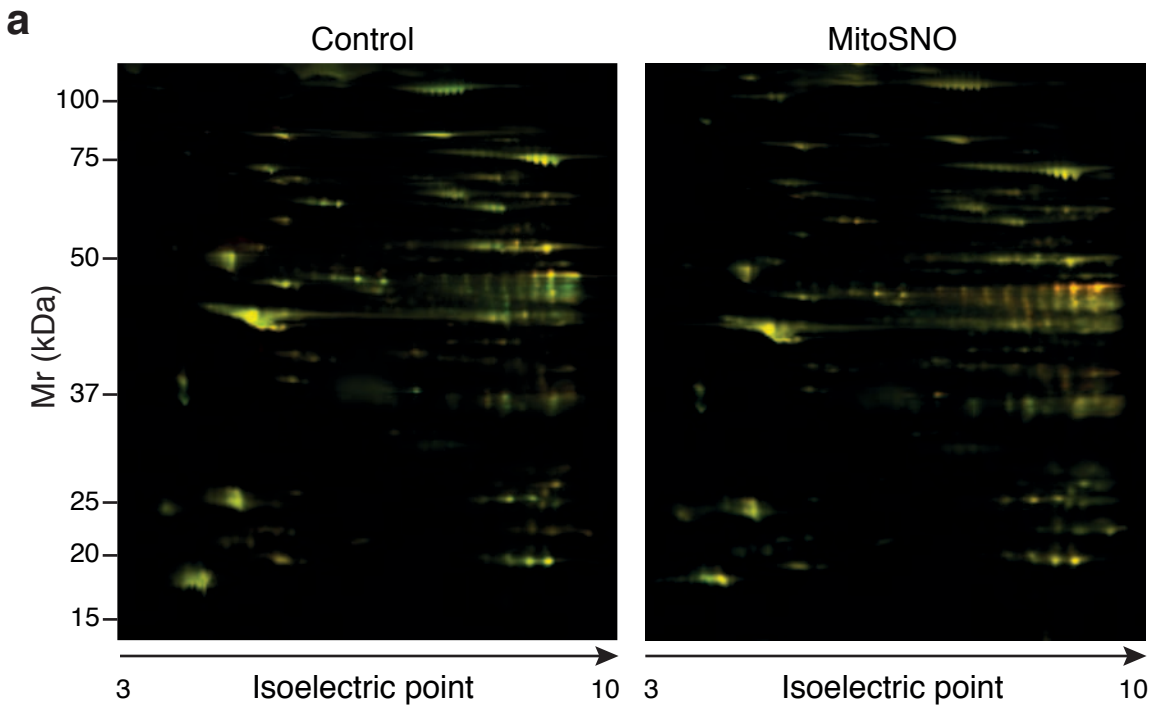

b

Parameter	Description	Data
Spots matched	Unique spots matched across at least 10 of 16 gels	1730
Cut-off	Volume ratio > 2, $p < 0.05$; between groups	0
Volume ratio SD	Standard deviation of fluorescence values	1.5

Fig. S5 Lack of broad *S*-nitrosation of mitochondrial proteins by MitoSNO within the intact heart.

a. Intact mouse hearts were perfused under anoxic conditions with MitoSNO and compared with hearts purfused in the absence of MitoSNO. After the perfusion, *S*-nitrosated mitochondrial thiols were selectively reduced and tagged with Cy5 maleimide (red), while all other oxidative modifications remained untagged. The Cy3 (green) labeled standard sample of mitochondrial proteins from a single heart replicate is pooled with the standard sample from four independent preparations and combined individually with the control and MitoSNO-treated Cy5 samples of every replicate sample (four control, four treated; eight in total). Combined samples are resolved by two-dimensional electrophoresis on the same gel and fluorescently scanned. Protein spots that appear red on the superimposed image of the treated gels (right) but not the control gels (left) have undergone MitoSNO-mediated *S*-nitrosation within the intact heart. Spots that appear yellow in both gels are equally oxidised in each preparation. The superimposed fluorescent scans of representative gels from each triplicate experimental condition are shown. Unlike the SDS-PAGE analysis shown in Fig. 1a, 2D proteomic determination of *S*-nitrosation events requires the use of a pooled standard Cy3 component to control for variability between gel preparations. **b**. Summary of proteomic analysis of *S*-nitrosated mitochondrial proteins in anoxic perfused hearts from four independent replicates indicating that MitoSNO causes negligible *S*-nitrosation of mitochondrial proteins within the intact heart. To ensure accurate comparison between gels and to allow for statistical analysis between groups, a threshold for inclusion required spot matching in at least 10 of 16 gels.

Supplementary Figure 6

a

Band	Complex Identified	Subunits identified	Unique peptides
C1	Complex I	28	103
CV	ATP Synthase	7	19

b

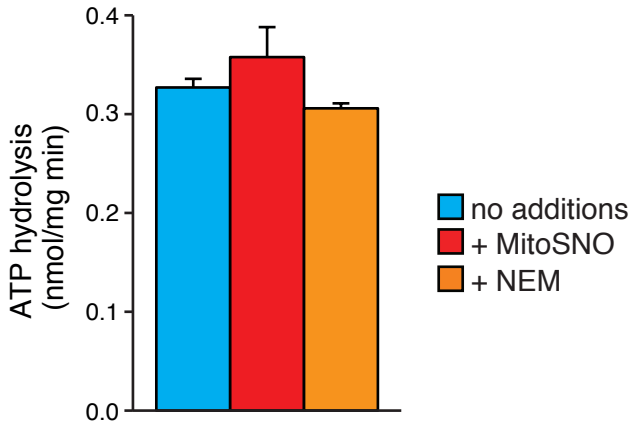

Fig. S6 MS identification of *S*-nitrosated respiratory complexes *in vivo* and impact of *S*-nitrosation on ATP synthase activity.

a, Mass spectrometric identification of the mitochondrial protein complexes *S*-nitrosated by MitoSNO *in vivo*. To confirm the identity of the two mitochondrial oxidative phosphorylation complexes that were *S*-nitrosated by MitoSNO and resolved by BN-PAGE in Fig. 1f, the bands exhibiting fluorescence were excised, resolved by SDS-PAGE and protein bands were excised and identified by Orbitrap MS/MS. The table summarizes the presence of intact complexes from these samples as determined by requiring the identification of the majority of their constituent subunits by MS/MS. The band referred to as C1 in Fig. 1f contains intact complex I as determined by identification of 28 subunits, while the CV band contains intact ATP synthase as determined by identification of 7 subunits. Samples were digested with trypsin. Full sequencing data is provided in Supplementary Table 1. **b**, S-nitrosation of the F_0F_1-ATP synthase by MitoSNO does not affect its activity, nor does alkylation of all surface cysteine residues with NEM. Mitochondrial membranes were incubated with no additions, with MitoSNO, or with NEM, and the ATP hydrolysis activity of F_0F_1-ATP synthase was determined. N=3 .

Supplementary Figure 7

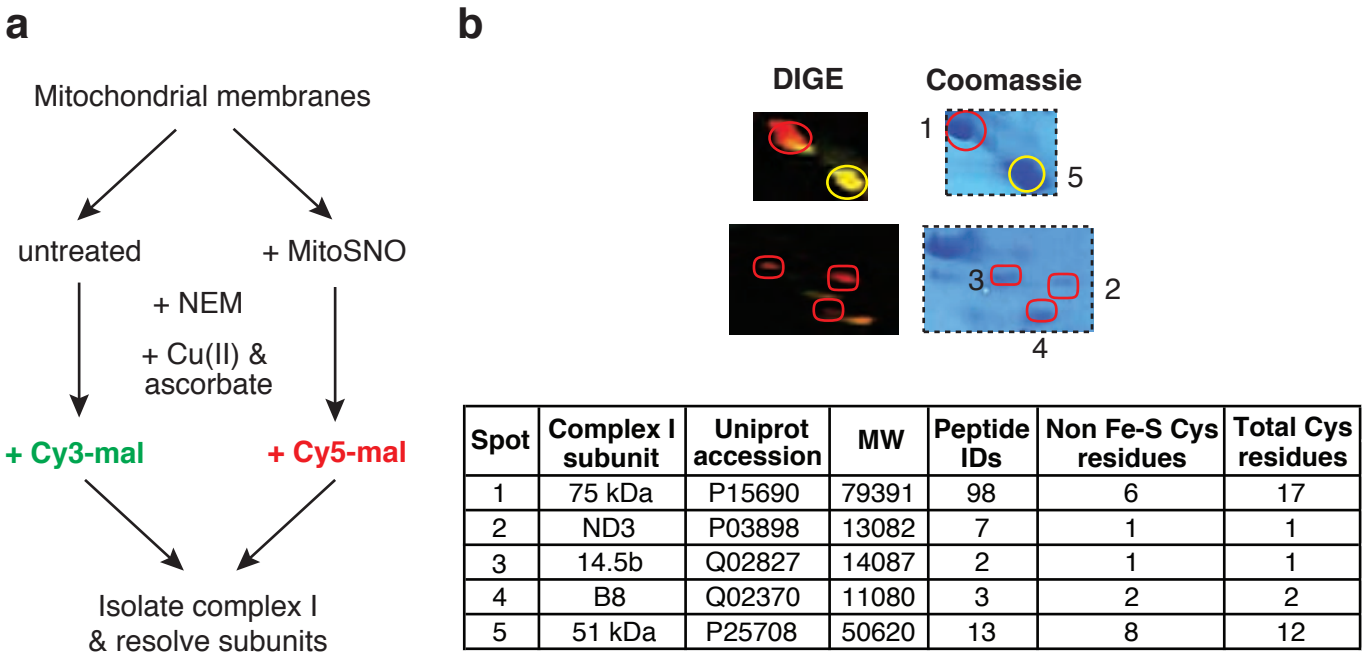

Spot	Complex I subunit	Uniprot accession	MW	Peptide IDs	Non Fe-S Cys residues	Total Cys residues
1	75 kDa	P15690	79391	98	6	17
2	ND3	P03898	13082	7	1	1
3	14.5b	Q02827	14087	2	1	1
4	B8	Q02370	11080	3	2	2
5	51 kDa	P25708	50620	13	8	12

Fig. S7 Fluorescent labeling of complex I subunits.
a, Mitochondrial membranes treated ± MitoSNO (50 μM) have unreacted cysteine thiols blocked with NEM followed by selective reduction and tagging of *S*-nitrosothiols in the presence of fluorescent cysteine-reactive maleimides. **b**, Fluorescent scan and Coomassie Blue stain of complex I subunits of interest. Spots highlighted in red contained *S*-nitrosated subunit(s) due to selective labeling with a red fluorescent cysteine-reactive dye. The spot highlighted in yellow is a representative subunit exhibiting equivalent red and green fluorescence due to labeling of occluded cysteine thiols. The Table shows the identification of complex I subunits by mass spectrometry. Full supporting mass spectrometry data are contained in Table S2.

Supplementary Figure 8

Nature Medicine doi:10.1038/nm.3212

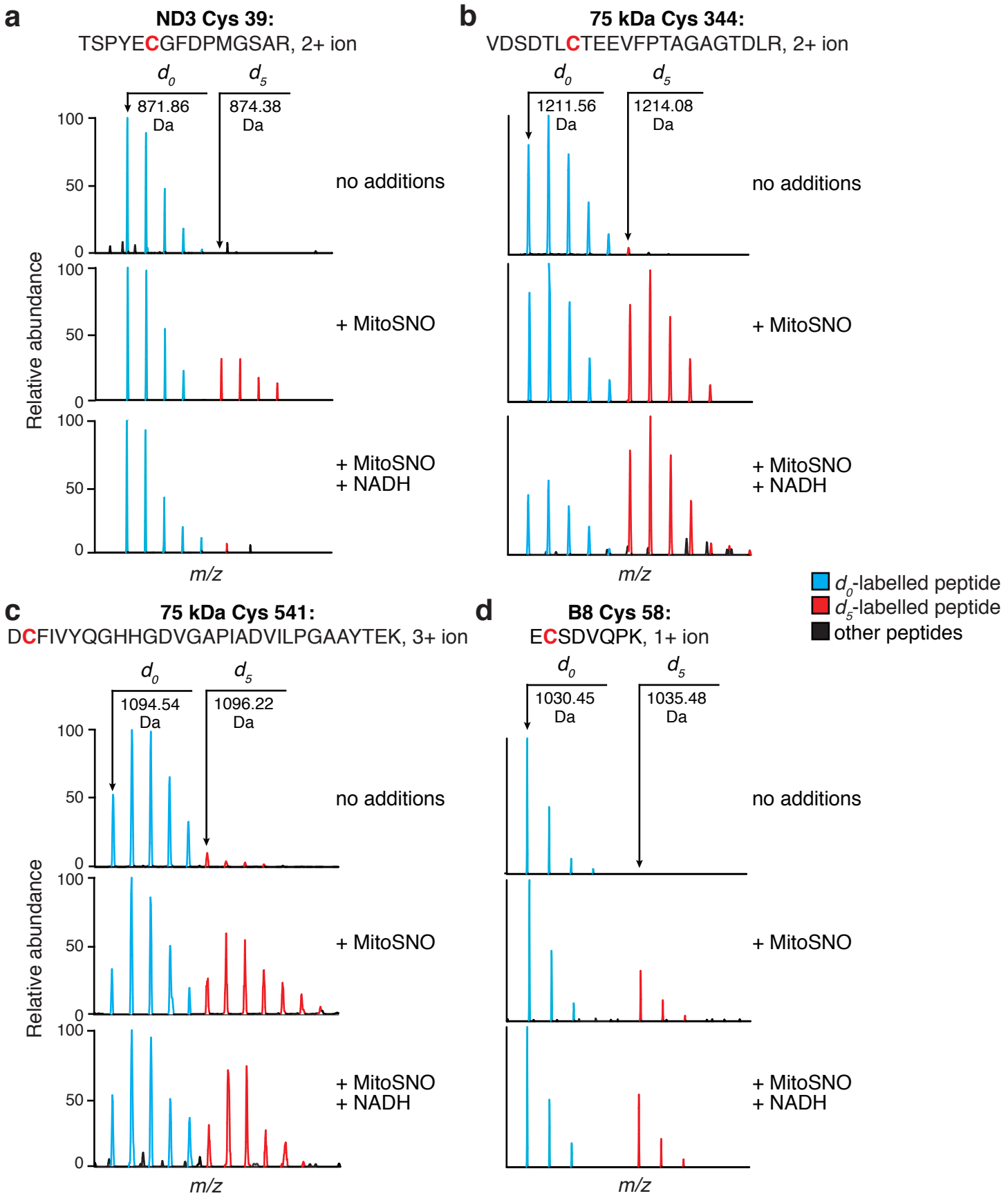

Fig. S9 Precursor ion mass spectra of ratiometrically labeled *S*-nitrosated cysteines within complex I. The d_0-labelled peptides that correspond to unmodified cysteine residues are highlighted in blue, while d_5-labeled peptides corresponding to *S*-nitrosated cysteines are highlighted in red. The relative intensity of these two forms allows for quantification of *S*-nitrosation, shown in Figs. 2 & 3. **a**, ND3 cys 39 *S*-nitrosation requires low complex I activity conditions, while for all other susceptible complex I cysteines *S*-nitrosation is independent of complex I activity (**b-d**). Peptide sequence, charge and mass are included.

Supplementary Figure 9

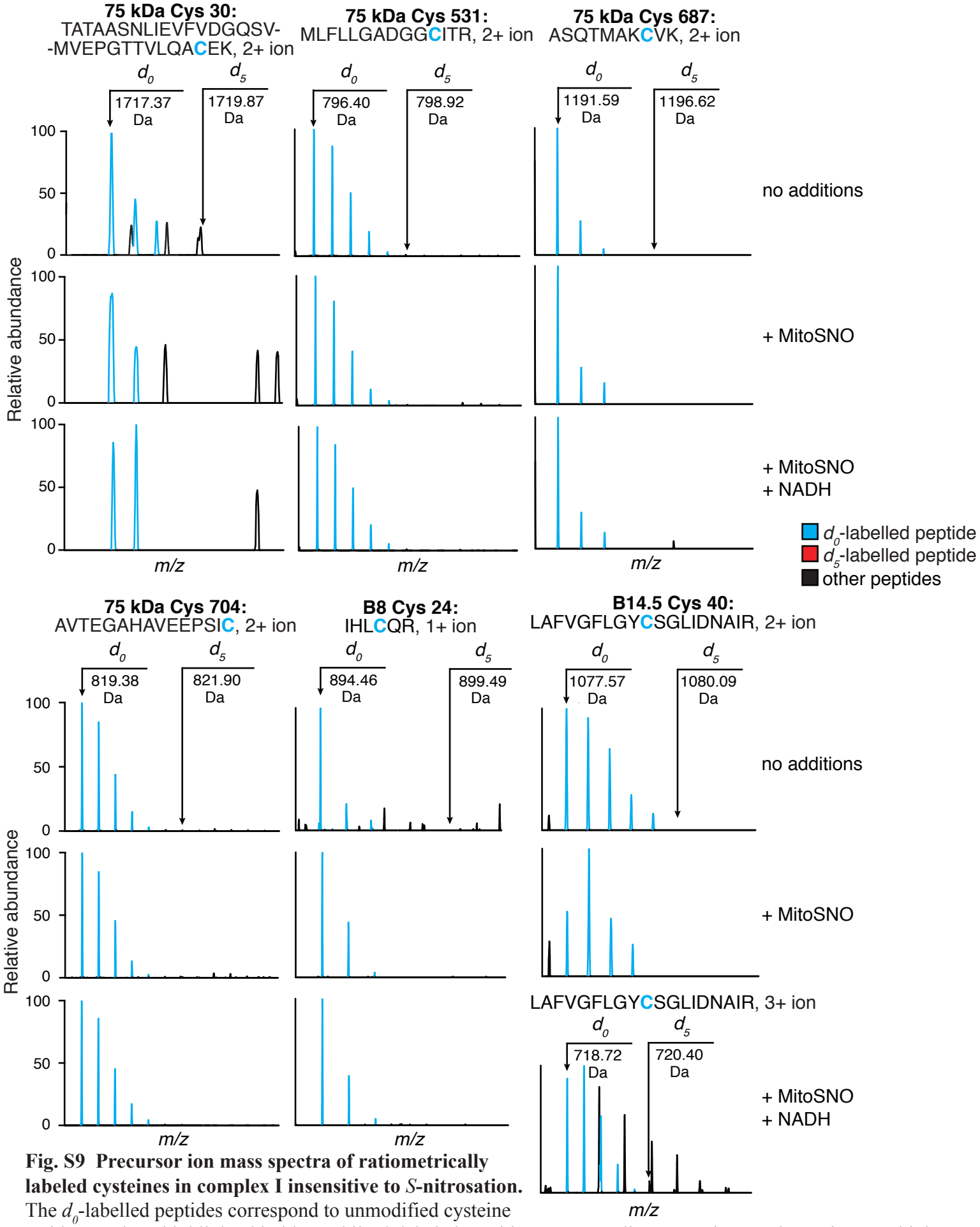

Fig. S9 Precursor ion mass spectra of ratiometrically labeled cysteines in complex I insensitive to *S*-nitrosation. The d_0-labelled peptides correspond to unmodified cysteine residues and are highlighted in blue, while d_5-labeled peptides corresponding to *S*-nitrosated cysteines are highlighted in red. Relative abundance of these two forms allows for quantification of *S*-nitrosation, shown in Fig. S10.

Supplementary Figure 10

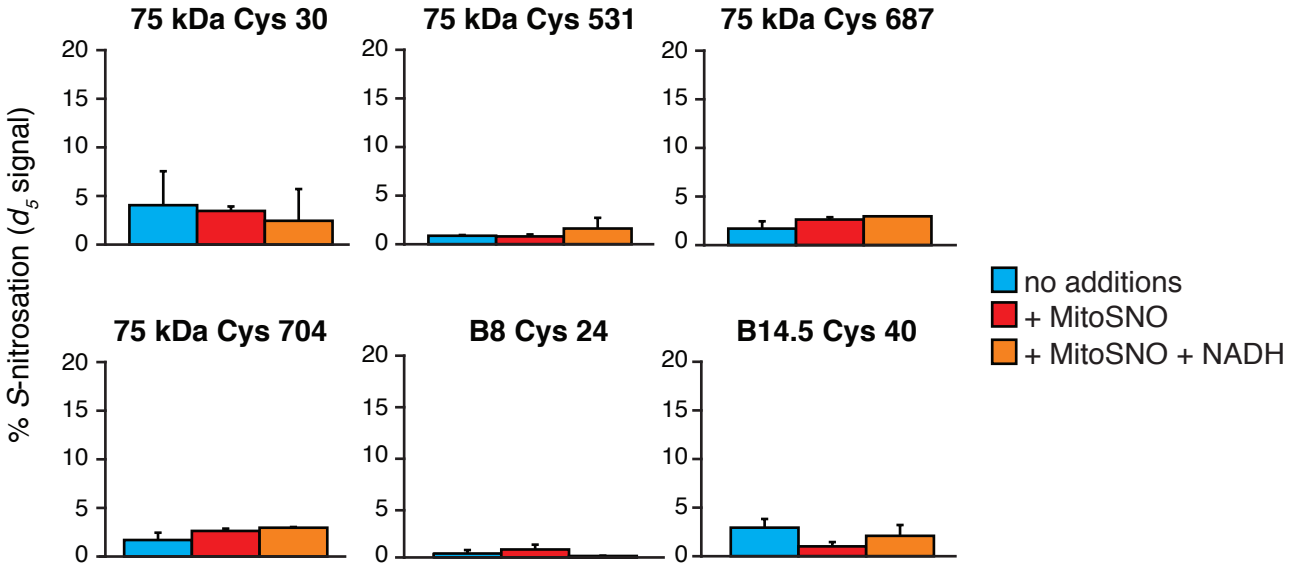

Fig. S10 Quantification of complex I cysteine *S*-nitrosation.
Ratiometric quantification of unmodified (d_0-labeled) and *S*-nitrosated (d_5-labeled) peptides for complex I cysteines contained within *S*-nitrosated subunits whose extent of *S*-nitrosation is insensitive to complex I activity. N = 3 for all peptides under all conditions.

Supplementary Figure 11

a

Subunit	Cys	Peptide	d_0-NEM MH+	d_5-NEM MH+	Ion
75 kDa	30	TTGTAASNLIEVFVDGQSVMVEPGTTVLQACEK	3520.72	3525.75	3
	344	VDSDNLCTEEIFPTEGAGTDLR	2507.12	2512.15	3
	531	MLFLLGADGGCITR	1591.80	1596.83	2
	541	DCFIVYQGHHGDVGAPMADVILPGAAYTEK	3299.55	3304.58	3
	687	ASQTMAKCVK	1191.59	1196.62	2
ND3	39	ANPYECGFDPTSSAR	1739.73	1744.76	2

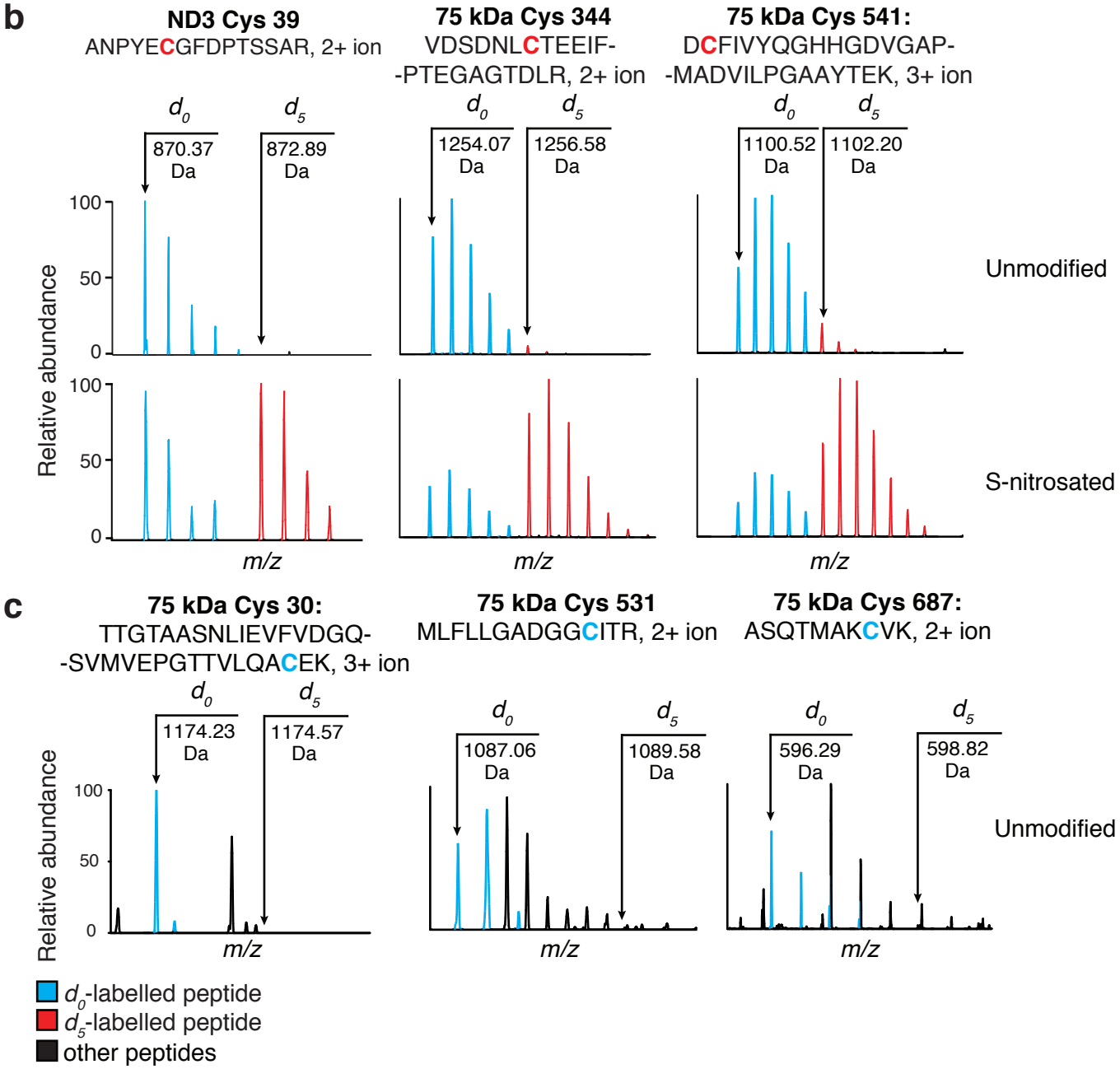

Fig. S11 Precursor ion masses of cysteine-containing peptides within *S*-nitrosated complex I subunits analyzed following treatment of mouse hearts with MitoSNO.

a, Cysteine-containing peptide sequences, masses and charges. **b**, Representative parent ion spectra of d_0-labeled (blue) and d_5-labeled (red) forms of cysteine-containing peptides sensitive to *S*-nitrosation. **c**, Representative parent ion spectra of d_0-labelled cysteine-containing peptides insensitive to *S*-nitrosation.

Nature Medicine doi:10.1038/nm.3212

Supplementary Figure 12

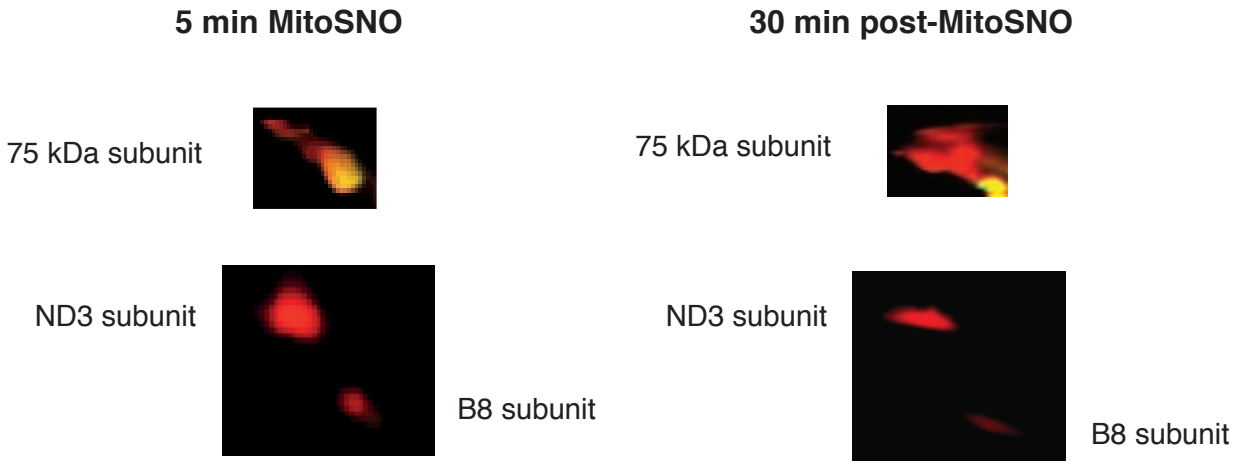

Fig. S12 Persistence of *S*-nitrosation of complex I subunits in mitochondrial membranes. Mitochondrial membranes containing complex I in an inactive form by incubation under anoxic conditions were incubated with MitoSNO for 5 min.The *S*-nitrosation of complex I subunits was then determined by labelling with a red fluorescent label followed by diagonal gel eletrophoresis as in Fig. 2a. Relevant regions of fluorescent-scanned diagonal SDS-PAGE gel demonstrates that 30 min post *S*-nitrosation the modification of the sensitive subunits is maintained (red fluorescent spots) due to the absence of a thiol reducing system in the mitochondrial membrane incubation.

Supplementary Figure 13

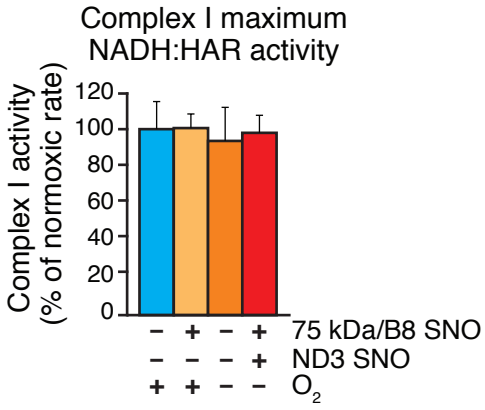

Fig. S13 Complex I NADH:hexaammine ruthenium activity is unaffected by ND3 cysteine 39 *S*-nitrosation.

Mitochondrial membranes were incubated under anaerobic or anoxic conditions ± MitoSNO, leading to a range of *S*-nitrosation patterns on complex I subunits, as indicated under the bar chart. The complex I NADH:hexaammine ruthenium activity was then determined. N = 3.

Supplementary Figure 14

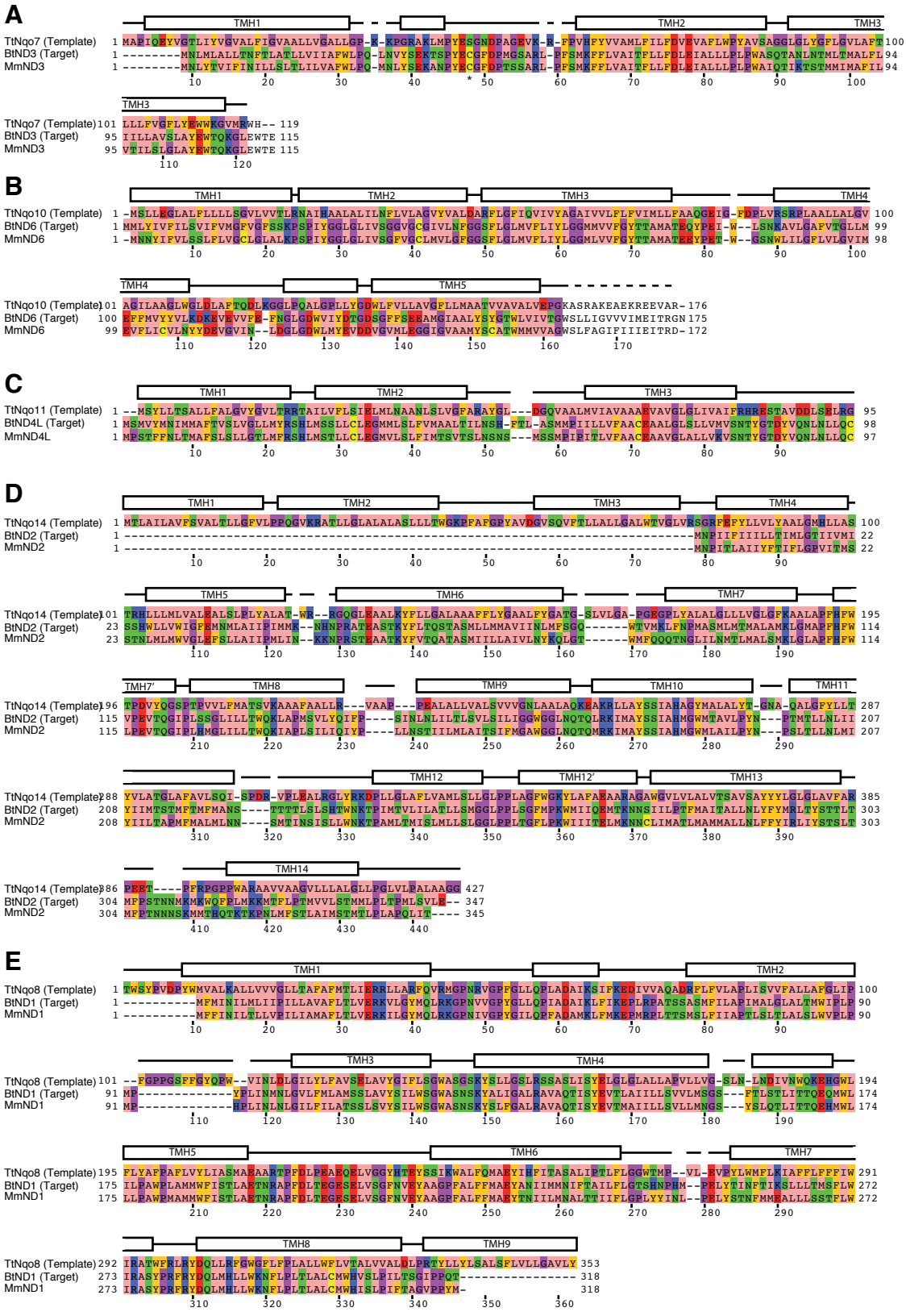

Fig S14: Sequence alignment of complex I core hydrophobic subunits. Pairwise sequence alignments of membrane subunits of bacterial complex I from Thermus thermophilus (Tt) with the orthologous sequences of mitochondrial complex I from *Bos taurus* (Bt) and *Mus musculus* (Mm). Secondary structure elements from the bacterial complex I are shown: α-helices (rectangles), loops (line), and unresolved structure (dashed line). The amino acids are coloured: basic (blue), acidic (red), polar (green), aromatic (orange), aliphatic (pink), glycine and proline (magenta), and cysteine (yellow). Residues that are unresolved in the template structure (*T. thermophilus*) or not modeled in the target structure (*B. taurus*) are not colored. (a) Nqo7 and ND3 subunits. Cysteine 39 is indicated (*). (b) Nqo10 and ND6 subunits. (c) Nqo11 and ND4L subunits. (d) Nqo14 and ND2 subunits. (e) Nqo8 and ND1 subunits.

Supplementary Figure 15

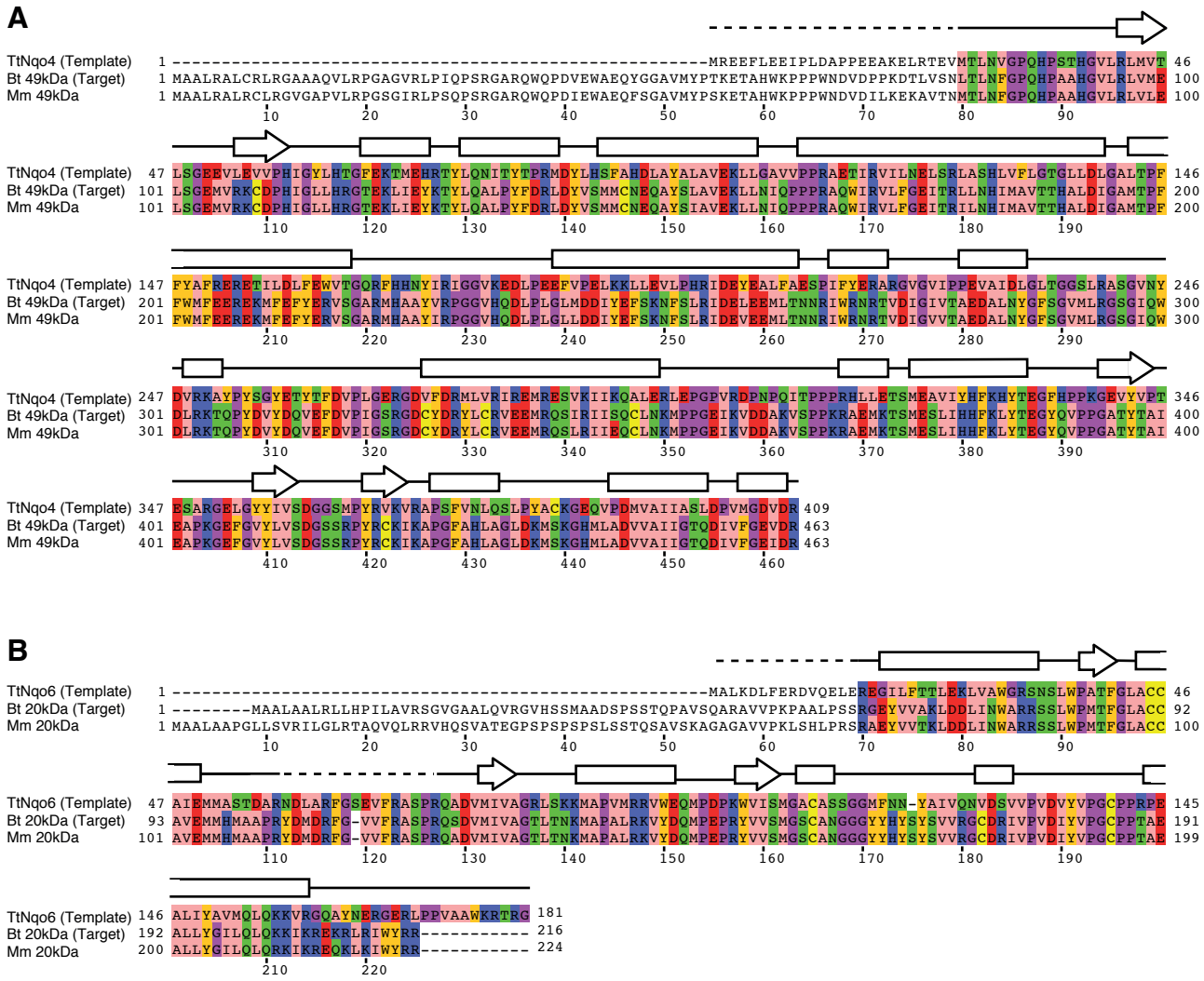

Fig. S15: Sequence alignment of complex I core hydrophilic subunits. Pairwise sequence alignments of hydrophilic subunits of bacterial complex I from *Thermus thermophilus* (Tt) with the orthologous sequences of mitochondrial complex I from *Bos taurus* (Bt) and *Mus musculus* (Mm). Secondary structure elements from the bacterial complex I are shown: α-helices (rectangles), β-strands (arrows), loops (line), and unresolved structure (dashed line). The amino acids are coloured: basic (blue), acidic (red), polar (green), aromatic (orange), aliphatic (pink), glycine and proline (magenta), and cysteine (yellow). Residues that are unresolved in the template structure (*T. thermophilus*) or not modeled in the target structure (*B. taurus*) are not colored. (a) Nqo4 and 49 kDa subunits. (b) Nqo6 and 20 kDa subunit.

Supplementary Figure 16

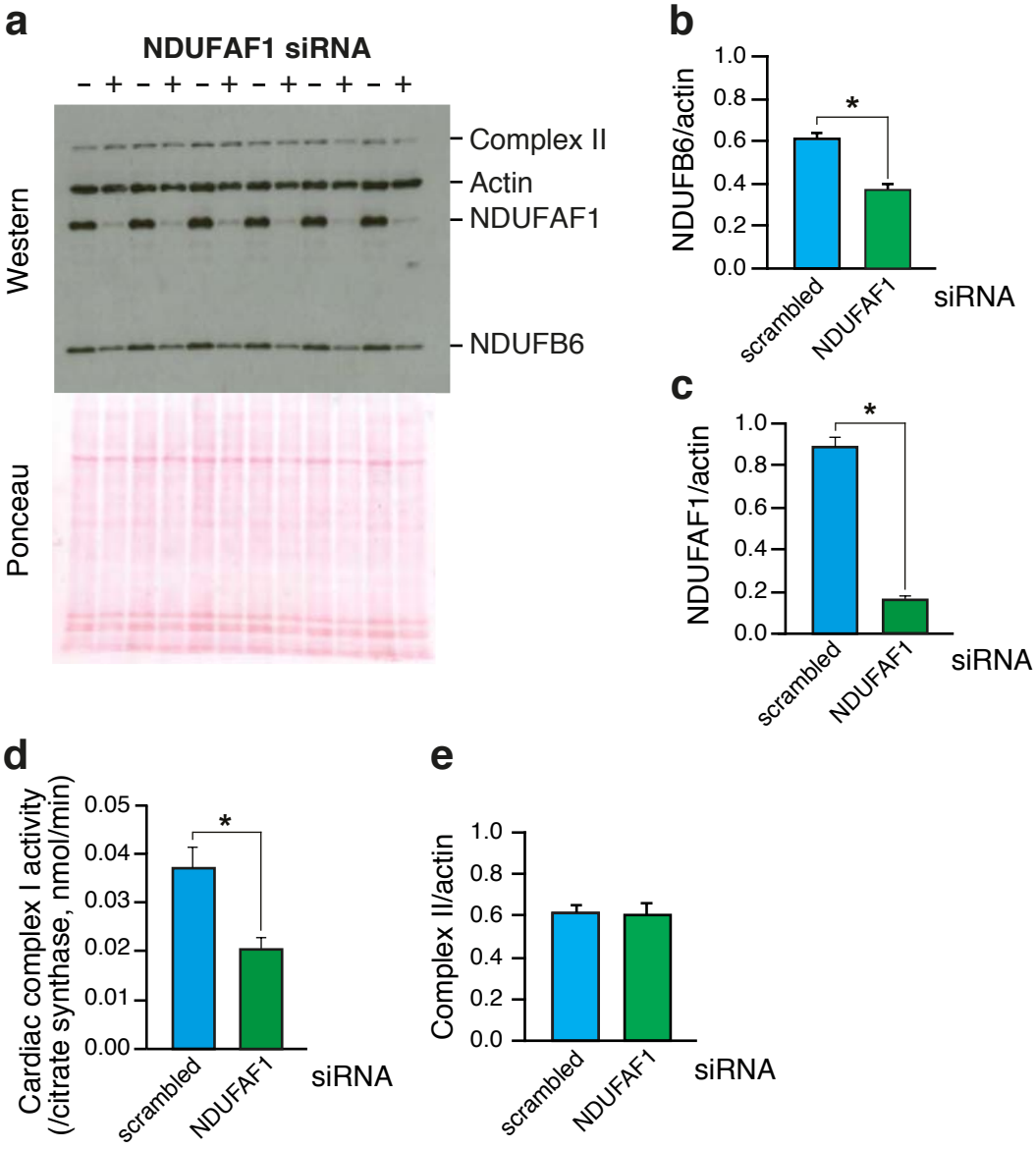

Fig. S16 Complex I deficiency in H9C2 cells generated by siRNA knockdown of NDUFAF1. H9C2 cells were incubated with siRNA against NDUFAF1 or a scrambled control siRNA. **a**, The level of expression of complex II, actin, NDUFAF1 and NDUFB6 were determined by western blotting. **b**, The level of NDUFB6 RNA relative to actin was determined by scanning densitometry. **c**, The level of complex II relative to actin was determined by scanning densitometry. N= 3, * $p < 0.05$.

Supplementary Figure 17

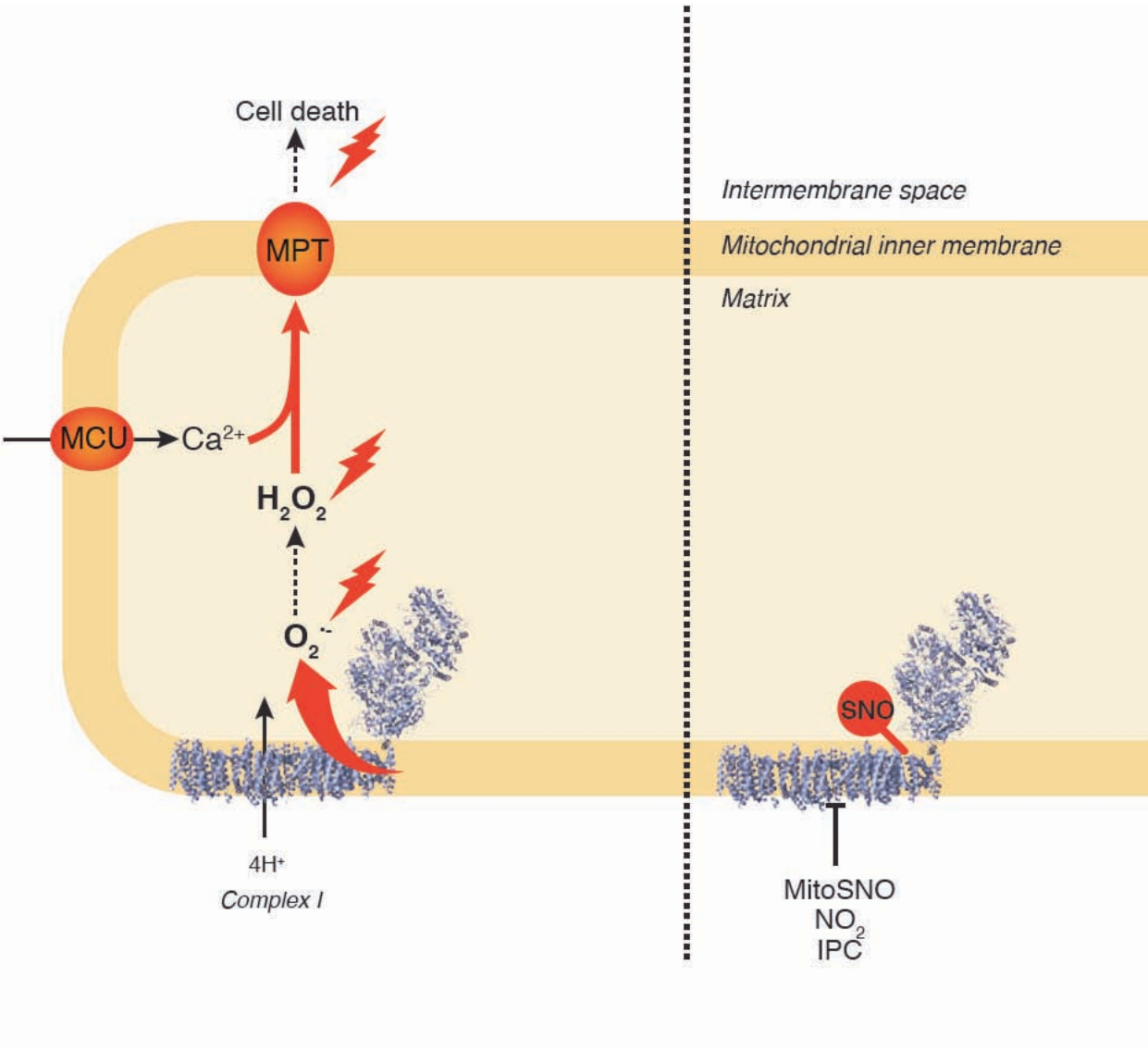

Fig. S17 A model for the role of complex I in IR injury and the prevention of this damage by *S*-nitrosation.

The left side of this schematic shows the situation during reperfusion after prolonged ischemia. In this context there is an elevated flux of mitochondrial H_2O_2 during reperfusion. The elevated H_2O_2 that in conjunction with the accumulation of calcium within mitochondria during ischemia goes on to induce the mitochondrial permeability transition (MPT) pore that leads to cell death. This is a major source of tissue damage in IR injury. On the right hand side of the schematic, we indicate how the conversion of complex I to its less active form by the *S*-nitrosation of ND3 cysteine 39 selectively decreases reverse electron transport and mitochondrial ROS production during IR injury. *S*-nitrosation can be brought about by MitoSNO, as shown in this work.

Table S1. Mass spectrometric sequencing summary of isolated intact respiratory complexes identified as targets of *S*-nitrosation *in vivo*. a, Peptide sequencing information for 27 complex I subunits was obtained following isolation and trypsin digestion of the CI band (Fig. 2f) confirming the identity of intact respiratory complex I. b, Peptide sequencing information for 7 ATP synthase subunits was obtained following isolation and trypsin digestion of the CV band (Fig. 2f) confirming the identity of intact ATP synthase. Only MASCOT scores above a significance threshold of $p < 0.05$ are included.

a

Uniprot Accession	Subunit	Peptides matched	MASCOT score
Q9CQ75	NDUFA2	6	211
Q9CQ91	NDUFA3	2	31
Q62465	NDUFA4	2	131
Q9CPP6	NDUFA5	3	141
Q9CQZ5	NDUFA6	4	134
Q9Z1P6	NDUFA7	2	69
Q9DCJ5	NDUFA8	6	154
Q9D8B4	NDUFA11	1	65
Q7TMF3	NDUFA12	2	53
Q9ERS2	NDUFA13	10	468
Q9CPU2	NDUFB2	1	36
Q9CQZ6	NDUFB3	5	153
Q9CQC7	NDUFB4	3	130
Q9CQH3	NDUFB5	5	164
Q3UIU2	NDUFB6	9	467
Q9CR61	NDUFB7	9	706
Q9D6J5	NDUFB8	8	420
Q9DCS9	NDUFB10	1	52
O09111	NDUFB11	9	596
Q9CQ54	NDUFC2	6	167
Q91VD9	NDUFS1	42	2407
Q9CXZ1	NDUFS4	2	58
Q8BK30	NDUFV3	1	56
P03888	ND1	1	29
P03899	ND3	1	33
P03911	ND4	3	86
P03921	ND5	2	51

b

Uniprot Accession	Subunit	Peptides matched	MASCOT score
P03930	ATP8	3	154
Q03265	alpha subunit	6	178
Q9D3D9	delta subunit	2	145
Q06185	subunit e	4	191
P56135	subunit f	2	112
Q9CPQ8	subunit g	3	269
P56382	subunit epsilon	2	34

Table S2 Mass spectrometric sequencing coverage of complex I subunits containing *S*-nitrosated cysteines. Samples were digested with either trypsin (T) or chymotrypsin (Ch). Only ions scores above a significance threshold of $p < 0.05$ are included.

Spot	Enzyme	Uniprot accession	Complex I subunit	Observed (MH+)	(delta)M (ppm)	Sequence	Modifications	Ions score
1	T	P15690	75 kDa	2121.08794	1.05	KTESIDVMDAVGSNIVVSTR		125
				2008.98584	0.08	TESIDVmDAVGSNIVVSTR	M7(Oxidation)	108
				2137.08136	0.34	KTESIDVmDAVGSNIVVSTR	M8(Oxidation)	107
				2121.0894	1.74	KTESIDVMDAVGSNIVVSTR		107
				1608.78846	1.23	FASEIAGVDDLGTTGR		106
				2137.08339	1.29	KTESIDVmDAVGSNIVVSTR	M8(Oxidation)	104
				2008.98766	0.99	TESIDVmDAVGSNIVVSTR	M7(Oxidation)	100
				1608.78839	1.19	FASEIAGVDDLGTTGR		95
				1555.84455	0.4	NDGAAILAAVSNIAQK		94
				2137.08387	1.51	KTESIDVmDAVGSNIVVSTR	M8(Oxidation)	90
				2008.98722	0.77	TESIDVmDAVGSNIVVSTR	M7(Oxidation)	90
				1992.99365	1.45	TESIDVMDAVGSNIVVSTR		87
				2109.05596	1.24	ALSEIAGmTLPYDTLDQVR	M8(Oxidation)	83
				1591.80015	1.86	MLFLLGADGGcITR	C11(NEM)	82
				2137.08318	1.19	KTESIDVmDAVGSNIVVSTR	M8(Oxidation)	81
				2093.06315	2.25	ALSEIAGMTLPYDTLDQVR		80
				1555.84516	0.79	NDGAAILAAVSNIAQK		80
				1385.71874	1.4	McLVEIEKAPK	C2(NEM)	79
				1599.81533	1.7	GLLTHTTWEDALSR		77
				2109.05633	1.41	ALSEIAGmTLPYDTLDQVR	M8(Oxidation)	74
				1661.71209	0.5	mHEDINEEWISDK	M1(Oxidation)	73
				2093.06533	3.3	ALSEIAGMTLPYDTLDQVR		73
				1403.79208	1.94	VALIGSPVDLTYR		73
				2137.08318	1.19	KTESIDVmDAVGSNIVVSTR	M8(Oxidation)	72
				2168.13996	2.43	ILQDIASGSHPFSQVLQEAK		72
				2422.11315	2.13	VDSDTLcTEEVFPTAGAGTDLR	C7(NEM)	71
				2171.20896	0.83	IASQVAALDLGYKPGVEAIQK		71
				1645.71856	1.35	MHEDINEEWISDK		70
				1607.79424	1.32	mLFLLGADGGcITR	M1(Oxidation) C11(NEM)	70
				2440.1236	2.07	VDSDTLcTEEVFPTAGAGTDLR	C7(NEMhyd)	70
				1609.81056	1.74	MLFLLGADGGcITR	C11(NEMhyd)	69
				1918.86272	1.39	mHEDINEEWISDKTR	M1(Oxidation)	69
				2758.46713	1.76	SNYLLNTTIAGVEEADVVLLVGTNPR		68
				1262.63115	0.41	VVAAcAMPVMK	C5(NEMhyd)	66
				1625.80632	2.24	mLFLLGADGGcITR	M1(Oxidation) C11(NEMhyd)	66
				1244.62097	0.72	VVAAcAMPVMK	C5(NEM)	65
				1385.71794	0.82	McLVEIEKAPK	C2(NEM)	64
				1403.79118	1.3	VALIGSPVDLTYR		63
				1992.99211	0.68	TESIDVMDAVGSNIVVSTR		62
				1655.76103	1.71	AVTEGAHAVEEPSIc	C15(NEMhyd)	61
				1370.62754	1.33	GNDmQVGTYIEK	M4(Oxidation)	61
				1403.79026	0.65	VALIGSPVDLTYR		60
				2109.05376	0.19	ALSEIAGmTLPYDTLDQVR	M8(Oxidation)	60
				2109.05474	0.66	ALSEIAGmTLPYDTLDQVR	M8(Oxidation)	60
				2171.20996	1.29	IASQVAALDLGYKPGVEAIQK		59
				2100.24884	2.87	LVNQQLLADPLVPPQLTIK		59
				1415.80394	-0.03	KPmVILGSSALQR	M3(Oxidation)	59
				1276.61144	1.19	VVAAcAmPVmK	C5(NEM) M7(Oxidation) M10(Oxidation)	57
				1415.80351	-0.33	KPmVILGSSALQR	M3(Oxidation)	57
				1555.84731	2.17	NDGAAILAAVSNIAQK		57
				1260.61692	1.53	VVAAcAMPVmK	C5(NEM) M10(Oxidation)	56
				1399.81028	0.87	KPMVILGSSALQR		56
				1370.626	0.21	GNDmQVGTYIEK	M4(Oxidation)	56
				1354.63286	1.52	GNDMQVGTYIEK		56
				1415.80309	-0.63	KPmVILGSSALQR	M3(Oxidation)	56
				1294.62089	0.32	VVAAcAmPVmK	C5(NEMhyd) M7(Oxidation) M10(Oxidation)	55
				1294.61968	-0.61	VVAAcAmPVmK	C5(NEMhyd) M7(Oxidation) M10(Oxidation)	55
				1645.71784	0.91	MHEDINEEWISDK		54
				1278.62612	0.44	VVAAcAMPVmK	C5(NEMhyd) M10(Oxidation)	54
				1155.63794	0.92	LEEVSPNLVR		54
				800.44611	1.67	VGMQIPR		53
				2171.21047	1.53	IASQVAALDLGYKPGVEAIQK		53
				1244.62041	0.27	VVAAcAMPVMK	C5(NEM)	53
				1260.61659	1.27	VVAAcAmPVMK	C5(NEM) M7(Oxidation)	53
				1425.78293	1.41	NRLEEVSPNLVR		52
				1637.74994	1.4	AVTEGAHAVEEPSIc	C15(NEM)	51
				882.4987	0.95	VMNILHR		50
				1234.54419	2.65	DFYMTDSISR		50
				1097.52375	1.4	SATYVNTEGR		50
				2109.05612	1.31	ALSEIAGmTLPYDTLDQVR	M8(Oxidation)	49
				1902.86835	1.69	MHEDINEEWISDKTR		49

Table S2 (continued)

Spot	Enzyme	Uniprot accession	Complex I subunit	Observed (MH+)	(delta)M (ppm)	Sequence	Modifications	Ions score
1	T	P15690	75 kDa	1250.53826	1.94	DFYmTDSISR	M4(Oxidation)	49
				2137.08329	1.24	KTESIDVmDAVGSNIVVSTR	M8(Oxidation)	49
				2137.08469	1.89	KTESIDVmDAVGSNIVVSTR	M8(Oxidation)	49
				2958.56354	0.97	VAGmLQSFQGNDVAAIAGGLVDAEALIALK	M4(Oxidation)	48
				1655.75866	0.28	AVTEGAHAVEEPSIc	C15(NEMhyd)	48
				1555.84636	1.56	NDGAAILAAVSNIAQK		48
				1064.55303	0.58	FEAPLFNAR		47
				1415.80509	0.79	KPmVILGSSALQR	M3(Oxidation)	47
				2093.06135	1.4	ALSEIAGMTLPYDTLDQVR		46
				1625.80425	0.97	mLFLLGADGGcITR		46
				969.51573	0.46	FAYDGLKR		46
				1031.47976	0.47	YDHLGDSPK		46
				816.44109	1.72	VGmQIPR	M3(Oxidation)	46
				1419.72335	0.75	mcLVEIEKAPK	M1(Oxidation) C2(NEMhyd)	45
				2422.11221	1.74	VDSDTLcTEEVFPTAGAGTDLR	C7(NEM)	45
				1031.47981	0.51	YDHLGDSPK		45
				2121.08823	1.18	KTESIDVMDAVGSNIVVSTR		44
				1294.62094	0.36	VVAAcAmPVmK	M10(Oxidation)	44
				3033.44933	0.73	DLLNRVDSDTLcTEEVFPTAGAGTDLR	C12(NEM)	44
				898.49323	0.5	VmNILHR	M2(Oxidation)	44
				882.49751	-0.4	VMNILHR		44
				1260.61503	0.03	VVAAcAMPVmK	C5(NEM) M10(Oxidation)	43
				944.46135	-0.55	LSVAGNcR	C7(NEM)	43
				2100.24479	0.95	LVNQQLLADPLVPPQLTIK		42
				1276.61081	0.7	VVAAcAmPVmK	C5(NEM) M7(Oxidation) M10(Oxidation)	42
				1637.74849	0.51	AVTEGAHAVEEPSIc	C15(NEM)	42
				2168.14267	3.68	ILQDIASGSHPFSQVLQEAK		42
2	Ch	P03898	ND3	861.44978	3.09	TQKGLEW		49
				1176.57256	3.49	EWTQKGLEW		44
				1106.53411	3.73	DPmGSARLPF	M3(Oxidation)	44
				861.44921	3.1	EWTQKGL		42
				1406.66411	3.82	EWTQKGLEWTE		31
				811.3856	2.91	SEKTSPY		30
				1091.54018	3.77	TQKGLEWTE		22
3	Ch	Q02827	14.5b	1345.6576	2.98	GEVFEEFHPVR		41
				1006.44396	2.8	AVRDHDmF	M7(Oxidation)	38
4	Ch	Q02370	B8	1415.75426	3.75	SADQVTRALENVL		46
				960.51319	2.35	SADQVTRAL		39
				1467.72966	4.72	AFGQEKNVSLNNF		32
4	Ch	Q02365	B12	1584.89054	3.88	KIEGTPLETVQEKL		48
				846.45951	3.25	ETVQEKL		40
5	T	P25708	51 kDa	1710.84922	2.68	GEFYNEASNLQVAIR		74
				1382.6974	4.55	KTSFGSLKDEDR		56
				1778.82958	4.52	NAcGSGYDFDVFVVR	C3(NEMhyd)	51
				1212.61808	4.97	HFRPELEER		44
				1055.50881	2.85	GGAWFASFGR		41
				983.53478	3.92	IFTNLYGR		41
				1372.6576	2.67	MQQFAQQHQAR		40
				1254.60066	3.61	TSFGSLKDEDR		39
				978.43785	2.91	EGVDWMNK		37
				1050.54729	0.61	EAYEAGLIGK		37
				2614.41275	5.3	HAGGVTGGWDNLLAVIPGGSSTPLIPK		35
				1388.65281	2.85	mQQFAQQHQAR	M1(Oxidation)	35
				1212.61729	4.32	HFRPELEER		25

Table S3 Mass spectrometric sequencing coverage of all cysteine-containing peptides within complex I subunits sensitive to *S*-nitrosation in their d_0-labelled form only (insensitive cysteines), or both d_0-labelled and d_5-labelled forms (sensitive to S-nitrosation) digested with trypsin.

Mass spectrometric sequencing data from membrane experiments using bovine material, as well as *in vivo* experiments using rat and mouse material are included. Only ions scores above the significance threshold of $p < 0.05$ are included. 75 kDa Cys 30 and Cys 687 were not sequenced, and identification in these cases was based on peptide mass fingerprinting alone.

Species	CI Subunit	Cys	Sequence	Modification	Theoretical mass	Measured mass	Expectation score	(delta)M (ppm)	Ions score	MS2 ions matched
Bovine	75 kDa	344	DLLNRVDSDTLCTEEVFPTAGAGTDLR	NEM	3033.4500	3033.4520	2.10E-06	1.60	64	22
		344	DLLNRVDSDTLCTEEVFPTAGAGTDLR	NEMhyd	3051.4577	3051.4634	4.30E-04	1.88	41	20
		344	DLLNRVDSDTLCTEEVFPTAGAGTDLR	d5-NEM	3038.4800	3038.4955	2.70E-03	5.60	44	16
		344	VDSDTLCTEEVFPTAGAGTDLR	NEM	2422.1100	2422.1183	2.40E-02	4.25	34	6
		344	VDSDTLCTEEVFPTAGAGTDLR	d5-NEM	2427.1400	2427.1524	1.10E-05	5.38	68	11
		344	VDSDTLCTEEVFPTAGAGTDLR	d5-NEMhyd	2445.1499	2445.1582	3.90E-04	3.40	53	8
		531	MLFLLGADGGCITR	NEM	1591.8000	1591.8051	4.90E-11	5.00	120	12
		531	MLFLLGADGGCITR	NEM, mOx	1607.7913	1607.8006	3.40E-06	5.42	33	15
		531	MLFLLGADGGCITR	NEMhyd	1609.8033	1609.8145	2.30E-05	4.19	63	10
		531	MLFLLGADGGCITR	NEMhyd, mOx	1625.8027	1625.8095	4.20E-05	4.20	61	10
		541	DCFIVYQGHHGDVGAPIADVILPGAAYTEK	NEM	3281.5900	3281.6000	1.10E-05	1.93	56	22
		541	DCFIVYQGHHGDVGAPIADVILPGAAYTEK	d5-NEM	3286.6200	3286.6428	6.70E-04	5.38	50	24
		541	DCFIVYQGHHGDVGAPIADVILPGAAYTEK	NEMhyd	3299.6040	3299.6085	8.60E-03	1.28	28	27
		704	AVTEGAHAVEEPSIC	NEM	1637.7476	1637.7545	1.20E-03	4.21	45	6
		704	AVTEGAHAVEEPSIC	NEMhyd	1655.7582	1655.7632	1.40E-03	3.00	45	21
Bovine	ND3	39	TSPYECGFDPMGSAR	NEM	1742.7200	1742.7140	2.80E-04	-0.53	63	18
		39	TSPYECGFDPMGSAR	NEMhyd, mOx	1776.7205	1776.7197	1.70E-03	-0.44	55	7
		39	TSPYECGFDPMGSAR	NEM, mOx	1758.7099	1758.7094	1.10E-03	-0.28	56	10
Bovine	B8	24	IHLCQR	NEM	894.4618	894.4601	1.00E+00	-1.51	16	7
		58	ECSDVQPK	NEM	1030.4513	1030.4505	3.40E-03	-0.49	34	7
Mouse	75 kDa	344	VDSDNLCTEEIFPTEGAGTDLR	NEM	2507.1200	2507.1276	3.80E-10	1.27	107	11
		344	VDSDNLCTEEIFPTEGAGTDLR	d5-NEM	2512.1500	2512.1589	3.90E-10	1.26	107	11
		531	MLFLLGADGGCITR	NEM	1591.8000	1591.7974	1.50E-05	0.14	62	13
		531	MLFLLGADGGCITR	NEM, mOx	1607.7900	1607.7917	4.90E-08	-0.29	86	12
		541	DCFIVYQGHHGDVGAPMADVILPGAAYTEK	NEM	3299.5500	3299.5557	9.50E-09	1.69	94	26
		541	DCFIVYQGHHGDVGAPMADVILPGAAYTEK	d5-NEM	3304.5800	3304.5874	1.80E-07	1.78	81	16
		704	AVTEGAQAVEEPSIC	NEM	1628.7500	1628.7495	1.40E-07	1.37	81	11
Rat, mouse	ND3	39	ANPYECGFDPTSSAR	NEM	1739.7300	1739.7364	9.10E-08	1.90	82	9
		39	ANPYECGFDPTSSAR	d5-NEM	1744.7600	1744.7647	7.40E-05	0.16	54	13

Table S4: The percentage *S*-nitrosation of sensitive complex I cysteines within the intact heart during normoxia and ischemia ± MitoSNO. *n* = 3–6 for all conditions, * P < 0.05, ** P < 0.01, versus normoxia untreated.

Subunit	Cys	Normoxia		Ischemia	
		Untreated	MitoSNO	Untreated	MitoSNO
75 kDa	30	< 1.9 ± 1.7	< 2.6 ± 1.2	< 2.3 ± 2.1	< 3.7 ± 3.2
	344	< 1.9 ± 1.6	37.2 ± 8.0 **	5.8 ± 0.7 *	18.8 ± 5.9 **
	531	< 3.6 ± 1.3	< 1.7 ± 1.0	< 3.3 ± 1.1	<1.5 ± 0.9
	541	< 0.9 ± 0.4	44.5 ± 8.7 **	< 4.8 ± 2.1	45.1 ± 11.2 **
	687	< 0.9 ± 0.9	< 2.8 ± 1.5	< 1.9 ± 0.7	< 0.9 ± 0.7
ND3	39	< 0.4 ± 0.2	< 3.3 ± 1.8	4.1 ± 2.2 *	37.8 ± 6.5 **

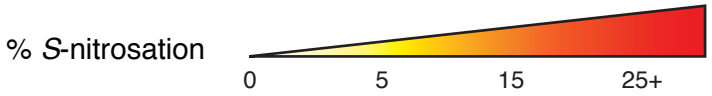

Table S5: Mass spectrometric sequencing identification of the Cys39 containing tryptic peptide of the ND3 subunit from *in vivo* gel experiments. For gel based experiments where ND3 *S*-nitrosation was studied by tagging with maleimide fluorophores, presence of the ND3 subunit was confirmed by MS sequencing of the ND3 Cys39 containing peptide. Representative sequencing data from these experiments are shown below. Only ions scores above the significance threshold of p < 0.05 are included.

Sequence	Modification	Theoretical mass	Measured mass	Expectation score	(delta)M (ppm)	Ions score	Ions matched	Reference exp
ANPYECGFDPTSSAR	NEM	1739.7300	1739.7326	1.00E-02	-0.26	33	7	Fig. 3b
ANPYECGFDPTSSAR	NEM	1739.7300	1739.7305	9.50E-06	-1.45	63	8	Fig. 3c
ANPYECGFDPTSSAR	NEM	1739.7300	1739.7313	8.40E-04	-1.03	44	8	Fig. 3c
ANPYECGFDPTSSAR	NEM	1739.7300	1739.7321	5.70E-05	-0.54	56	7	Fig. 4b
ANPYECGFDPTSSAR	NEM	1739.7300	1739.7344	3.00E-02	0.79	29	10	Fig. 4b

Table S6: Ratiometric labeling of complex I cysteine *S*-nitrosothiols with d_5-NEM in hearts subjected to IPC. *n* = 3–6 for all conditions, * P < 0.05, ** P < 0.01, versus normoxia untreated.

Subunit	Cys	Untreated	IPC
75 kDa	30	< 1.9 ± 1.7	< 1.1 ± 0.6
	344	< 1.9 ± 1.6	33.2 ± 13.6 **
	531	< 3.6 ± 1.3	< 2.5 ± 0.8
	541	< 0.9 ± 0.4	48.5 ± 22.9 *
	687	< 0.9 ± 0.9	< 1.2 ± 1.0
ND3	39	< 0.4 ± 0.2	21.1 ± 8.9 *

SUPPLEMENTARY METHODS

***In vivo* treatments.** To assess the effects of MitoSNO on hemodynamics, mice were placed in a Plexiglass induction chamber filled with 3% isoflurane in O_2. Adequacy of anesthesia was confirmed through testing of the pedal reflex. Animals were moved to a warmed surgical platform, intubated and ventilated with 2% isoflurane in O_2 (0.125 ml tidal volume, 240 breaths/min) using a positive end-expiratory pressure ventilator (Hugo Sachs Electronik-Harvard Apparatus, Germany). Body temperature was monitored using a rectal thermometer and maintained at 37ºC via an animal temperature controller (TCAT-2LV, Physitemp, USA). The left ventricle was catheterized with a 1.2 F Pressure Conductance Catheter (SciSense Inc., Canada) in a closed-chest approach as described previously[1]. Briefly, using a dissection microscope (Mantis Compact, Vision Engineering, UK) a small mid-line incision was made in the neck and the right carotid artery was exposed and isolated from the vagus nerve. A 4/0 USP suture was secured tightly around the proximal end of the artery. A second suture was placed loosely at the distal end of the arterial section and a vascular clamp (0.4-1 mm) fixed close to the distal suture to minimize blood loss. A small incision was made near the proximal end of the artery with microincision scissors, and the pressure catheter inserted into the vessel. The catheter was then extended down into the left ventricle such that it lay parallel to the long axis and positioned until good peaks were observed. Data output was via a FV896B rodent pressure-volume control unit (SciSense Inc., Canada) and laptop using LabScribe2 software (SciSense Inc., Canada). Following left ventricular catheterization, hemodynamics were allowed to stabilize for 15 min before a 100 µl bolus of either vehicle or drug solution was given as an intravenous (IV) injection into the tail vein. Parameters including heart rate, left ventricular pressure (LVP), dP/dt_{max} and dP/dt_{min} (maximum and minimum rate of pressure change in the left ventricle over time; indices of ventricular performance), were recorded for a further 15 min. A section of ten stable pressure peaks were selected and averaged to determine mean basal values. Further sections were selected as close to indicated time points as possible post IV injection (30 s, 1, 2, 3, 4, 5, 10 and 15 min). In the case of an unstable period of peaks, a larger section of data was selected for averaging. Results are expressed as a mean percentage change in relation to basal values unless otherwise stated. Animals with a dP/dt_{max} of <5000 mm Hg/s following the stabilization period or animals in which hemodynamics were not sufficiently stable to determine basal values were excluded. All animals were sacrificed upon completion of the experimental protocol via cervical dislocation.

Fractionation of myocardial cytosolic fraction. Cytosolic proteins from myocardial tissue was isolated using Qproteome Cell Compartment Kit (Qiagen) according to the manufacturer's instructions. All buffers were supplemented with 100 mM NEM and fractionation was performed in the dark.

Measurement of ATP synthase activity. Following treatments (control, 75 µM MitoSNO, or 50 mM NEM), mitochondrial membranes containing 200 µg protein were washed in 10 mM HEPES, 120 mM KCl, 1 mM EDTA, 1 mM DTPA, and 10 µM neocuproine, pH 7.4, before resuspension in assay buffer consisting of 100 mM Tris, 50 mM KCl, 2 mM $MgCl_2$, 0.2 mM EDTA, pH 8 (HCl). ATP hydrolysis was measured as described previously[2] using an enzyme assay coupling ATP synthase activity to NADH consumption by exogenous lactate dehydrogenase through pyruvate kinase.

Hydrogen peroxide measurement using Amplex Red. The production of H_2O_2 upon reoxygenation *in vitro* was obtained by incubating mitochondrial membranes or mitochondria under anoxic conditions for 25 min, then adding 10 M MitoSNO or MitoNAP for the final 5 min of anoxia before reoxygenation was induced by pelleting the mitochondria or membranes by centrifugation and then resuspending in oxygenated buffer containing fresh respiratory substrate, 0.5 mM ADP, and Amplex Red assay components. H_2O_2 production was tracked spectrophotometrically by monitoring the oxidation of Amplex Red to resorufin at 585 nm[3]. Samples subjected to *in vitro* anoxia- reoxygenation were compared to samples treated in parallel at normoxia for 30 min.

Measurement of protein carbonyl content. Ischemic heart tissue from *in vivo* treatments were snap-frozen in liquid nitrogen and were stored at –80˚C. The tissues were then extracted and were assayed for protein carbonyl content using the Protein Carbonyl Enzyme Immuno-Assay Kit (BioCell Corp) according to the manufacturer's guidelines.

Measurement of apoptosis activation. Mice were anesthetized with inhaled isoflurane (3% induction, 2% maintenance), and exposed to 30 min cardiac ischemia as described above. After onset of reperfusion, the thoracic incision was closed and mice were monitored until recovery. Buprenorphine (0.05 mg/kg) was given subcutaneously just prior to the end of the surgery and during the recovery period if needed. Left ventricle samples containing the IR-treated tissue were collected 24 h after myocardial infarction. The expression of caspase 3 and cleaved caspase 3 (Cell Signaling Technology, 1:1000 dilution for each, 9662 and 9661) was analyzed by standard Western blotting techniques. The band intensity of three independent experiments was measured using SigmaGel software and normalized to GAPDH (Cell Signaling Technology, 1:1000 dilution, 2118).

Comparative modeling of subunits of the bovine mitochondrial complex I. The structure of bacterial complex I from *Thermus thermophilus*[4] was used to produce a comparative model of bovine complex I for analyzing the environment of Cys39 from the ND3 subunit. (Use of mouse sequences generated an essentially identical model). The ND3 subunit of mitochondrial complex I is orthologous to subunit Nqo3 of bacterial complex I. In the membrane domain of bacterial complex I, Nqo3 is in contact with the membrane subunits Nqo8, Nqo10, Nqo11 and Nqo14[5,6], which are orthologous to the mitochondrial complex I subunits ND1, ND6, ND4L and ND2 respectively. In the model of the complete bacterial complex I, Nqo3 is neighboring the subunits Nqo4 and Nqo6 of the hydrophilic domain, which are orthologous to the mitochondrial complex I subunits 49 kDa and 20 kDa. The protein sequences of these complex I subunits from *T. thermophilus* and *Bos taurus* were downloaded from UniProt[7]. The bacterial protein sequences were edited to remove amino acids that are not resolved in the molecular structures. MUSCLE[8] and manual editing was used to align each pair of orthologous sequences. To improve the quality of the comparative models, by using Jalview[9], the alignments were edited first to remove the N- and C-terminal residues of the bovine sequences that do not align with sequences resolved in the bacterial structures, and second to place gaps in the bovine sequences such that the distance between these residues in the initial target structure were minimal. By using the MODELLER program[10], the alignments and subunits of bacterial complex I were used to produce 50 comparative models of the orthologous subunits in bovine complex I. The structures of the

comparative models were examined and figures produced by using the PyMOL molecular visualization system (The PyMOL Molecular Graphics System, Version 1.4.1, Schrödinger, LLC.).

Cell culture and transfection. Cardiac derived H9C2 cells were grown in Complete Growth Media (CGM) comprising of DMEM, 4 mM glutamine, 10% FBS, and 1% penicillin/streptomycin. Cells were kept in the incubator at 37ºC equilibrated with 5% CO_2, and were used between passages 27-33. 24 h prior to transfection, cells were plated at 30,000/well on 22-mm 12-well plates (Greiner Bio-One) in antibiotic-free media. After 24 h, half the wells were transfected with 50 nM NDUFAF1 siRNA (QIAGEN, Valencia CA; #SI01602251) using lipofectamine RNAiMAX reagent (Invitrogen) according to the manufacturer's instructions. The other half was transfected with scrambled (negative) siRNA (#1027281). After 72 h, all the wells in a plate were assessed by either Western blotting, *in vitro* IR, or complex I/citrate synthase activity assays.

Verification of the successful gene silencing by RNAi was monitored by Western blotting as described previously[11] with minor modifications. Briefly, proteins were separated on 16.5% reducing SDS-PAGE, and transferred to nitrocellulose membrane. After Ponceau staining, the membrane was cut in four horizontal sections (Supplementary Figure 16a): (i) from the top of the membrane to ~50 kDa was probed with 70 kDa complex II antibodies (1:10000; MitoScience-Abcam Cambridge, MA); (ii) from ~50-37 kDa was probed for actin (1:10000; Calbiochem/EMD Gibbstown, NJ); (iii) from ~37-25 kDa was probed for NDUFAF1 (1:1000; Novus Littleton, CO); (iv) from ~25k Da to the bottom of the membrane was probed for NDUFB6 (1:1000; MitoScience-Abcam Cambridge, MA). Densitometry of the bands was performed using Scion Image software.

SUPPLEMENTARY METHODS REFERENCES

1. Pacher, P., Nagayama, T., Mukhopadhyay, P., Bátkai, S. & Kass, D. A. Measurement of cardiac function using pressure-volume conductance catheter technique in mice and rats. *Nat. Prot.* **3**, 1422-1434 (2008).
2. Pullman, M. E., Penefsky, H. S., Datta, A. & Racker, E. Partial resolution of the enzymes catalysing oxidative phosphorylation. I. Purification and properties of soluble dinitrophenol-stimulated adenosine triphosphatase. *J Biol Chem* **235**, 3322-3329 (1960).
3. Zhou, M., Diwu, Z., Panchuk-Voloshina, N. & Haugland, R. P. A stable nonfluorescent derivative of resorufin for the fluorometric determination of trace hydrogen peroxide: applications in detecting the activity of phagocyte NADPH oxidase and other oxidases. *Anal. Biochem.* **253**, 162-168 (1997).
4. Baradaran, R., Berrisford, J.M., Minhas, G.S. & Sazanov, L.A. Crystal structure of the entire respiratory complex I. *Nature* **494**, 443-448 (2013).
5. Efremov, R. G., Baradaran, R. & Sazanov, L. A. The architecture of respiratory complex I. *Nature* **465**, 441-445 (2010).
6. Efremov, R. G., Sazanov, L. A. Structure of the membrane domain of respiratory complex I. *Nature* **476**, 414-420 (2011).
7. UniProt Consortium. Ongoing and future developments at the Universal Protein Resource. *Nucleic Acids Res* **39**, D214 (2011).

8. R. C. Edgar, MUSCLE: multiple sequence alignment with high accuracy and high throughput. *Nucleic Acids Res* **32**, 1792 (2004).
9. A. M. Waterhouse, J. B. Procter, D. M. Martin, M. Clamp, G. J. Barton, Jalview Version 2--a multiple sequence alignment editor and analysis workbench. *Bioinformatics* **25**, 1189 (2009).
10. N. Eswar *et al.*, Comparative protein structure modeling using Modeller. *Curr Protoc Bioinformatics* **Chapter 5**, Unit 5 6 (2006).
11. Nadtochiy, S. M. *et al.* Nitroalkenes confer acute cardioprotection via adenine nucleotide translocase 1. *J. Biol. Chem.* **287**, 3573-3580 (2012).